SIAM J. APPL. MATH.
Vol. 77, No. 6, pp. 2136–2155

PERIODIC TRAVELING WAVES GENERATED BY INVASION IN CYCLIC PREDATOR–PREY SYSTEMS: THE EFFECT OF UNEQUAL DISPERSAL*

JAMIE J. R. BENNETT† AND JONATHAN A. SHERRATT†

Abstract. Periodic traveling waves (wavetrains) have been an invaluable tool in the understanding of spatiotemporal oscillations observed in ecological data sets. Various mechanisms are known to trigger this behavior, but here we focus on invasion, resulting in a predator–prey-type interaction. Previous work has focused on the normal form reduction of PDE models to the well-understood λ-ω equations near a Hopf bifurcation, though this is valid only when assuming an equal rate of dispersion for both predators and prey—an unrealistic assumption for many ecosystems. By relaxing this constraint, we obtain the complex Ginzburg–Landau normal form equation, which has a one-parameter family of periodic traveling wave solutions, parametrized by the amplitude. We derive a formula for the wave amplitude selected by invasion before investigating the stability of the solutions. This gives us a complete description of small-amplitude periodic traveling waves in the governing model ecosystem.

Key words. dispersal, periodic traveling waves, predator–prey, reaction–diffusion, cyclic populations, wavetrain, diffusion, Hopf bifurcation, stability

AMS subject classifications. 35C07, 35K57, 76E15, 92D40

DOI. 10.1137/16M1107188

1. Introduction.

It is well known that populations can cycle under certain ecological conditions, meaning there are temporal oscillations in abundance. Mathematical modeling has provided insight into the mechanisms that drive cyclic behavior [41], though the spatial nature of the process is less well understood. In some cases, cyclic populations oscillate uniformly across their habitat, but spatiotemporal patterning is also well documented [1, 17, 40] and has been known to severely disrupt some ecosystems. As an example, North America has an ongoing problem with spatially heterogeneous cyclic mountain pine beetle outbreaks that spread through and destroy vast areas of woodland. In the Rocky Mountain region of British Columbia alone, approximately 17 million acres of forest were infested by mountain pine beetles in 2004 compared to 0.4 million in 1999 [45], with impacts ranging from fire hazards to changes in the carbon cycle [12].

One important type of spatiotemporal patterning is periodic traveling waves (PTWs); peaks in population density move across the domain with constant shape and speed. In field data, such a pattern might manifest itself via peak and trough population densities being observed simultaneously at different locations—the two locations would appear to oscillate out of phase. Spatiotemporal data is difficult and costly to obtain, but there are a number of data sets that provide evidence of periodic traveling wave phenomena [17, 26, 38]. For instance, data has been collected on

*Received by the editors December 8, 2016; accepted for publication (in revised form) June 28, 2017; published electronically November 30, 2017.
http://www.siam.org/journals/siap/77-6/M110718.html
Funding: The first author's work was supported by The Maxwell Institute Graduate School in Analysis and Its Applications, a Centre for Doctoral Training funded by the UK Engineering and Physical Sciences Research Council (grant EP/L016508/01), the Scottish Funding Council, Heriot-Watt University, and the University of Edinburgh.
†Department of Mathematics and Maxwell Institute for Mathematical Sciences, Heriot-Watt University, Edinburgh EH14 4AS, UK (jjb1@hw.ac.uk, j.a.sherratt@hw.ac.uk).

larch budmoth populations demonstrating that waves in budmoth population density propagate across the Swiss Alps at an estimated speed of 210 km per year toward the northeast [4]. To be clear, these waves are not a result of individuals migrating across the landscape at 210 km per year but are a consequence of the governing cyclic nature of the budmoth's overall population, coupled with an intrinsic spatial dependence of the individuals. The same phenomenon is observed in oscillatory chemical reactions such as the BelousovZhabotinsky reaction [9].

The mathematical theory of PTWs has been instrumental in the understanding of waves observed in cyclic populations. A PTW is defined mathematically as a periodic function of both (one-dimensional) space and time. We model our populations using a set of partial differential equations; spatial terms are added to a set of coupled ordinary differential equations with a (stable) limit cycle. If a PTW solution exists for a given model, general theory implies that there exists a family of possible solutions [25], of which one is selected by imposed initial and boundary conditions that correspond to a particular ecological situation. This means one can know all parameter values in a model but be unable to predict the characteristics of PTWs seen in practice. It is, therefore, instructive to focus both on one specific type of ecological interaction and one pattern-generating scenario relevant to that interaction.

In this paper, we focus on predator–prey interactions. There are a number of ecological situations one could consider in a predator–prey system that would generate PTWs, including heterogeneous habitats [4, 13], hostile boundaries [31], migration driven by pursuit and evasion [3], and an invasion of alien species [23]. In this paper, we consider the latter of these mechanisms. Geographic features such as oceans, mountains, and forests prevent the interaction of species in different locations. Natural events can cause these divides to be bypassed, but humans especially are responsible for the introduction of foreign species today [7, 39]. Understanding invasions and the behavior left in their wake is therefore of considerable practical importance.

We model the predator–prey interaction in one space dimension using a reaction–diffusion system. Let $\mathbf{Y}(x,t) \in \mathbb{R}^2$ represent predator and prey population densities dependent on space, x, and time, t. A general two-species predator–prey system can be written as

$$\frac{\partial \mathbf{Y}}{\partial t} = \mathbf{F}(\mathbf{Y};\mu) + \mathbf{D}\frac{\partial^2 \mathbf{Y}}{\partial x^2}, \tag{1}$$

where $\mathbf{D}$ is a constant, diagonal 2×2 matrix of diffusion coefficients and $\mathbf{F} : \mathbb{R}^2 \to \mathbb{R}^2$ is a function describing the interaction. Typically, $\mathbf{F}$ will involve a number of ecological parameters, but we focus on one of them that we denote μ, so that we may control whether $d\mathbf{Y}/dt = \mathbf{F}$ has a limit cycle. Figure 1 illustrates how PTWs can be generated by an invasion in (1), with $\mathbf{F}$ specified using the well-known Rosenzweig–MacArthur model [27]. In this case, the generated waves are stable, but for some parameter values they may be unstable and will evolve into spatiotemporal irregularity.

Cyclic behavior arises as a result of a Hopf bifurcation associated with $\mathbf{F}$, which we assume is supercritical, giving rise to a stable limit cycle. In this paper, we show how one can derive analytic results about waves behind invasion using the theory of normal forms, a valid approximation close to a supercritical Hopf bifurcation. When close to the bifurcation point, waves have a small amplitude with near-sinusoidal oscillations, and so one can consider a simpler yet topologically equivalent set of normal form equations. From the viewpoint of applications, the restriction to small-amplitude waves is a severe limitation since most ecological studies are concerned with

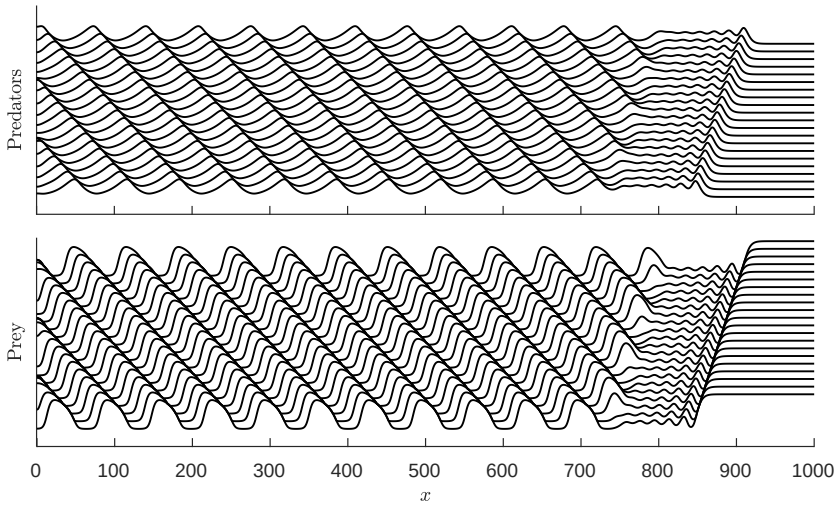

FIG. 1. *An illustration of invasion of predators into prey for cyclic populations. Numerical solutions of* (18) *are plotted as functions of space, x, at successive times, t. The vertical separation between plots is proportional to the time interval, with time increasing up the plot. Advancing and receding wave fronts of predator and prey, respectively, move from left to right, behind which is a band of periodic traveling waves. Parameter values are $A = 2$, $B = 3$, $C = 5$, $\delta = 1$; initial conditions correspond to a prey-only state everywhere except for a small perturbation at the left-hand boundary.*

large amplitude cycles. However, the generation of large-amplitude periodic traveling waves remains an open problem mathematically, and the study of small-amplitude waves provides an important framework for the interpretation of simulation-based studies of the larger-amplitude case. Previous work on small-amplitude cycles has focused on the special case where $\mathbf{D} = \mathbf{I}$, for which the normal form can be written as

$$\frac{\partial u}{\partial t} = (1 - r^2)u + \alpha r^2 v + \frac{\partial^2 u}{\partial x^2}, \qquad \frac{\partial v}{\partial t} = (1 - r^2)v - \alpha r^2 u + \frac{\partial^2 v}{\partial x^2}, \tag{2}$$

with $r^2 = u^2 + v^2$, an equation of λ-ω type first described by Kopell and Howard [14]. α is an expression containing the original model parameters in (1) and is determined via a normal form calculation that we will describe in section 2. Kopell and Howard showed that (2) have a one-parameter family of PTW solutions of the form

$$u = r_0 \cos\left(\pm\sqrt{1 - r_0^2}x - \alpha r_0^2 t\right), \qquad v = r_0 \sin\left(\pm\sqrt{1 - r_0^2}x - \alpha r_0^2 t\right), \tag{3}$$

for all r_0 such that $0 \leq r_0 \leq 1$. Furthermore, they showed that the generated waves are linearly stable as a solution of (2) if and only if

$$2(1 - r_0^2)(1 + \alpha^2) - r_0^2 \leq 0. \tag{4}$$

Sherratt [29] derived an amplitude formula for PTWs generated by invasion in the λ-ω equations,

$$r_0 = \left[\frac{2}{\alpha^2}\left(\sqrt{1 + \alpha^2} - 1\right)\right]^{\frac{1}{2}}, \tag{5}$$

which, together with (3) and (4), give a complete description of low-amplitude waves generated by invasion in a predator–prey model given by (1) with $\mathbf{D} = \mathbf{I}$.

In section 2, we review the theory of normal forms, showing that the normal form of (1) for general $\mathbf{D}$ is the cubic complex Ginzburg–Landau equation, giving explicit formulae for its coefficients. One way of obtaining the λ-ω normal form equations is to have $\mathbf{D} = \mathbf{I}$, implying that predator and prey dispersal rates are equal (an unrealistic assumption in many ecosystems). We prove the existence of alternative model constraints for a normal form reduction of λ-ω type in section 3, allowing one to study the effects of unequal dispersal using the established theory detailed in this section. The most general case is considered thereafter; in particular, a formula for the wave amplitude is derived for PTWs generated by invasion in the complex Ginzburg–Landau equations in section 4, allowing us to draw conclusions about stability in sections 5 and 6. This work allows us to study small-amplitude PTWs for general $\mathbf{F}$ and $\mathbf{D}$, i.e., for any model in the form (1). In section 7, we illustrate our results via an example.

2. Normal form coefficients: A review. There is a large, well-established volume of work that involves reducing (1) in the absence of diffusion to a topologically equivalent "normal" form under the assumption of small-amplitude limit cycles [10, 16]. This corresponds to being close to a Hopf bifurcation parameter in order to obtain near-sinusoidal oscillations. We consider solutions of (1) that are close in parameter space to this homogeneous oscillatory solution. Kuramoto [15] uses a method of multiple scales applied to space and time variables in order to reduce (1) to normal form. The Stuart–Landau equations are first derived for the homogeneous solution before results are extended to include diffusion terms. We give a brief review of the calculation, but a complete and detailed treatment can be found in Kuramoto's book.

Let us assume that $\mathbf{Y_0}(\mu)$ is a homogeneous steady state of (1) so that $\mathbf{F}(\mathbf{Y_0}(\mu); \mu) = 0$. One can express (1) in terms of $\mathbf{u} = \mathbf{Y} - \mathbf{Y_0}$ as a Taylor series expansion,

$$\frac{\partial \mathbf{u}}{\partial t} = \left(\mathbf{J} + \mathbf{D}\frac{\partial^2}{\partial x^2}\right)\mathbf{u} + \mathbf{Muu} + \mathbf{Nuuu} + \dots, \tag{6}$$

where $\mathbf{J}$ is the standard Jacobian matrix evaluated at $\mathbf{Y_0}$. $\mathbf{Muu}$ and $\mathbf{Nuuu}$ denote quadratic and cubic terms in $\mathbf{u}$, respectively, where the ith element is given by

$$(\mathbf{Muu})_i = \frac{1}{2!}\sum_{j,k}\left.\frac{\partial^2 F_i}{\partial Y_j \partial Y_k}\right|_{\mathbf{Y}_0} u_j u_k, \quad (\mathbf{Nuuu})_i = \frac{1}{3!}\sum_{j,k,l}\left.\frac{\partial^3 F_i}{\partial Y_j \partial Y_k \partial Y_l}\right|_{\mathbf{Y}_0} u_j u_k u_l. \tag{7}$$

$\mathbf{M}$ is sometimes referred to as the Hessian matrix. We denote elements of vectors using subscripts so that, for example, F_i is the ith element of $\mathbf{F}$. The stability of $\mathbf{Y_0}$ for space-independent perturbations is determined by the eigenvalues associated with $\mathbf{J}$. We let $\lambda(\mu) = \sigma(\mu) + i\omega(\mu)$ denote an eigenvalue that is becoming critical with complex conjugate, $\overline{\lambda}(\mu)$, and beyond the critical parameter value, μ_{crit}, the steady state, $\mathbf{Y_0}$, becomes unstable, generating a limit cycle in the homogeneous system. For the nonhomogeneous case, we assume the same—that instability is a result of a complex conjugate pair of eigenvalues associated with $\mathbf{J}$ becoming purely imaginary at μ_{crit}. In assuming this, we are neglecting the possibility of diffusion-driven instability, i.e., Turing patterns.

Near μ_{crit}, one can expand the quantities defined above in terms of a convenient parameter we label ε,

$$\begin{aligned} &\mathbf{u} = \varepsilon\mathbf{u_1} + \varepsilon^2\mathbf{u_2} + \dots, \qquad \mathbf{J} = \mathbf{J_0} + \varepsilon^2\chi\mathbf{J_1} + \varepsilon^4\mathbf{J_2} + \dots, \\ &\lambda = \lambda_0 + \varepsilon^2\chi\lambda_1 + \varepsilon^4\lambda_2 + \dots, \quad \mathbf{M} = \mathbf{M_0} + \varepsilon^2\chi\mathbf{M_1} + \varepsilon^4\mathbf{M_2} + \dots, \\ &\mathbf{N} = \mathbf{N_0} + \varepsilon^2\chi\mathbf{N_1} + \varepsilon^4\mathbf{N_2} + \dots, \end{aligned} \tag{8}$$

where $\varepsilon^2\chi = (\mu - \mu_{\text{crit}})$, $\chi = \text{sgn}(\mu - \mu_{\text{crit}})$, and $\lambda_\nu = \sigma_\nu + i\omega_\nu$. χ is introduced here because we have not yet specified whether a limit cycle is generated for $\mu < \mu_{\text{crit}}$ or $\mu > \mu_{\text{crit}}$, and so we ensure that ε is always well defined. The quantities $\mathbf{J_0}$, $\mathbf{M_0}$, and $\mathbf{N_0}$ are the matrices $\mathbf{J}$, $\mathbf{M}$, and $\mathbf{N}$, respectively, evaluated at μ_{crit}. Our assumptions imply that $\sigma_0 = 0$ in order to ensure that eigenvalues associated with the homogeneous linearized problem are purely imaginary when $\mu = \mu_{\text{crit}}$. Let $\mathbf{U}$ and $\mathbf{U}^*$ be right and left eigenvectors, respectively, associated with $\mathbf{J_0}$ and the eigenvalue λ_0. Then $\lambda_0 = i\omega_0 = \mathbf{U}^*\mathbf{J_0}\mathbf{U}$ and

$$\lambda_1 = \sigma_1 + i\omega_1 = \mathbf{U}^*\mathbf{J_1}\mathbf{U}. \tag{9}$$

We have used the fact that the eigenvectors are normalized such that $\mathbf{U}^*\mathbf{U} = \bar{\mathbf{U}}^*\bar{\mathbf{U}} = 1$, where a bar denotes a complex conjugate. Also, note the standard relationship $\mathbf{U}^*\bar{\mathbf{U}} = \bar{\mathbf{U}}^*\mathbf{U} = 0$.

The eigenvalue λ has a small real part of order ε^2, and so we introduce a scaled time variable defined by $\tau = \varepsilon^2 t$. A slow space dependence is also anticipated due to the slow spatiotemporal dynamics close to the Hopf bifurcation point, and so we write $\mathbf{u} = \mathbf{u}(t, \tau, s)$, scaling space as $s = \varepsilon x$. It can then be shown [15] by substitution of (8) into (6) that $\mathbf{Y}(t, \tau, s)$ is approximated close to the Hopf bifurcation point by the equation

$$\mathbf{Y}(t, \tau, s) = \mathbf{Y_0} + \varepsilon\left(W(\tau, s)e^{i\omega_0 t}\mathbf{U} + \bar{W}(\tau, s)e^{-i\omega_0 t}\bar{\mathbf{U}}\right),$$

where $W(\tau, s)$ is some complex amplitude that satisfies the unscaled complex Ginzburg–Landau equation

$$\frac{\partial W}{\partial \tau} = \chi\lambda_1 W - g|W|^2 W + d\frac{\partial^2 W}{\partial s^2}, \tag{10}$$

$$\text{with} \quad d = \mathbf{U}^*\mathbf{D}\mathbf{U}, \tag{11a}$$

$$\text{and} \quad g = -2\mathbf{U}^*\mathbf{M_0}\mathbf{U}\mathbf{V_0} - 2\mathbf{U}^*\mathbf{M_0}\bar{\mathbf{U}}\mathbf{V_+} - 3\mathbf{U}^*\mathbf{N_0}\mathbf{U}\mathbf{U}\bar{\mathbf{U}}, \tag{11b}$$

where $\mathbf{V_+} = -(\mathbf{L_0} - 2i\omega_0)^{-1}\mathbf{M_0}\mathbf{U}\mathbf{U}$ and $\mathbf{V_0} = -2\mathbf{L_0}^{-1}\mathbf{M_0}\mathbf{U}\bar{\mathbf{U}}$. The real and imaginary parts of W represent predator and prey population densities. With this result, we have outlined the calculations necessary to obtain the normal form coefficients (9) and (11), so that close to a Hopf bifurcation, one can reduce (1) to (10). Notice that (10) has no dependence on the control parameter μ due to the scalings we have made in space and time. We can further reduce the equation to the scaled complex Ginzburg–Landau equation (CGLE)

$$\frac{\partial W}{\partial \tau} = W - (1 + i\alpha)\left|W\right|^2 W + (1 + i\beta)\frac{\partial^2 W}{\partial s^2}, \tag{12}$$

where

$$\alpha = \frac{\text{Im}(g)}{\text{Re}(g)}, \quad \beta = \frac{\text{Im}(d)}{\text{Re}(d)}. \tag{13}$$

One obtains (12) by performing the change of variables:

$$\tau \to \frac{1}{\sigma_1}\tau\ , \quad s \to \sqrt{\frac{\mathrm{Re}(d)}{\sigma_1}}s\ , \quad W \to \sqrt{\frac{\sigma_1}{|\,\mathrm{Re}(g)|}}e^{\frac{i\omega_1}{\sigma_1}\tau}W. \tag{14}$$

All predator–prey models of the form (1) can be reduced to (12) with the assumptions detailed above, and so we can now safely focus our attention on the CGLE with the knowledge that results are related directly via (14).

In general, a predator–prey model of the form (1) gives nonzero α and β. However, in some special cases, one can obtain $\beta = 0$, and then (12) is simply the λ-ω equations (2), for which the results outlined in section 1 apply. Note that in this scenario, any diffusion coefficients in the original model are scaled out via (14). We now consider what features of (1) result in $\beta = 0$ and, hence, a normal form of λ-ω type.

3. Conditions for equations of λ-ω type. Predator–prey interactions in which populations tend to move about their habitats at similar rates can be represented in our model ecosystem by setting the dispersal coefficient of the predator population equal to that of the prey, i.e., $\mathbf{D} = \mathbf{I}$. This is appropriate for many aquatic micro-organisms [11], but the ratio of predator to prey dispersal rates will be significantly greater than one for most mammalian systems [5] and, also, for macroscopic marine species [44]. When $\mathbf{D} = \mathbf{I}$, one can clearly see that (11a) collapses to $d = \mathbf{U}^*\mathbf{I}\mathbf{U} = 1$ and implies $\beta = 0$ in (12), yielding λ-ω-type equations (2). We now show that $\mathbf{D} = \mathbf{I}$ is sufficient but not necessary in order to obtain equations of λ-ω form, allowing one to study the effects of unequal diffusion using theory described in section 1. We prove the following theorem:

THEOREM 3.1. *Consider* (1) *and let* $\mathbf{F}(\mathbf{Y};\mu) := (F_1(\mathbf{Y};\mu), F_2(\mathbf{Y};\mu))^T$ *be such that populations represented by* $\mathbf{Y}(x,t) := (Y_1(x,t), Y_2(x,t))^T$ *are cyclic as a result of a supercritical Hopf bifurcation. A normal form reduction then yields equations of* λ-ω *type if at least one of the following conditions hold:*

(i) $\mathbf{D} = \mathbf{I}$,

(ii) $$\left.\frac{\partial F_1}{\partial Y_1}\right|_{\mathbf{Y_0},\mu_{crit}} = \left.\frac{\partial F_2}{\partial Y_2}\right|_{\mathbf{Y_0},\mu_{crit}} = 0.$$

Proof. For $\beta = 0$, we need $\mathrm{Im}(d) = 0$. We consider equation (11a) and write $\mathbf{U}$, $\mathbf{J_0}$, and $\mathbf{D}$ in terms of their components:

$$\mathbf{U} := \begin{pmatrix} u_1 + iv_1 \\ u_2 + iv_2 \end{pmatrix}, \quad \mathbf{J_0} := \begin{pmatrix} j_1 & j_2 \\ j_3 & j_4 \end{pmatrix}, \quad \mathbf{D} := \begin{pmatrix} \delta_1 & 0 \\ 0 & \delta_2 \end{pmatrix},$$

where u_1, u_2, v_1, v_2, j_1, j_2, j_3, j_4, δ_1, $\delta_2 \in \mathbb{R}$. Note that since $\mathbf{J_0}$ is at criticality, i.e., $\mu = \mu_{crit}$, we express the purely complex eigenvalues associated with $\mathbf{J_0}$ as

$$\lambda, \bar{\lambda} = \pm i\sqrt{j_1 j_4 - j_2 j_3}, \tag{15}$$

$$\text{with} \quad j_1 j_4 - j_2 j_3 > 0 \quad \text{and} \quad j_1 + j_4 = 0. \tag{16}$$

The left eigenvalue $\mathbf{U}^*$ can be calculated in terms of u_1, u_2, v_1, v_2 so that (11a) implies

$$d = \frac{1}{2(u_1v_2 - u_2v_1)} \begin{pmatrix} v_2 + iu_2 \\ -v_1 - u_1 \end{pmatrix}^T \begin{pmatrix} \delta_1 & 0 \\ 0 & \delta_2 \end{pmatrix} \begin{pmatrix} u_1 + iv_1 \\ u_2 + iv_2 \end{pmatrix},$$

the imaginary part of which can be written as

$$\mathrm{Im}(d) = \frac{1}{2} \frac{(u_1u_2 + v_1v_2)(\delta_2 - \delta_1)}{(u_1v_2 - u_2v_1)}.$$

For $\mathrm{Im}(d) = 0$, we require $\delta_1 = \delta_2$ (i.e., $\mathbf{D} = \mathbf{I}$), or

$$u_1u_2 + v_1v_2 = 0. \tag{17}$$

One can easily show that the eigenvectors associated with $\mathbf{J_0}$ and (15) are given by

$$j_2(u_2 + iv_2) = \left(i\sqrt{j_1j_4 - j_2j_3} - j_1\right)(u_1 + iv_1),$$
$$j_3(u_1 + iv_1) = \left(i\sqrt{j_1j_4 - j_2j_3} - j_4\right)(u_2 + iv_2).$$

Without loss of generality, choose $u_1 + iv_1 = j_2$ and $u_2 + iv_2 = i\sqrt{j_1j_4 - j_2j_3} - j_1$. Then (17) implies that $j_1j_2 = 0$. Together with (16), we have $j_1 = 0$ and $j_4 = 0$ with either $j_2 < 0$ and $j_3 > 0$, or $j_2 > 0$ and $j_3 < 0$. Note that $j_2 \neq 0$ because (16) would not be satisfied. Recall that $\mathbf{J_0}$ is simply the Jacobian matrix evaluated at both $\mathbf{Y} = \mathbf{Y_0}$ and $\mu = \mu_c$. ∎

We have discussed Theorem 3.1(i) and its ecological significance. We now provide an example of a widely used predator–prey model for which Theorem 3.1(ii) applies.

Example: The Rosenzweig–MacArthur model. In order to reduce the number of parameters that need to be considered, we present the well-known Rosenzweig–Macarthur model [27] in its nondimensionalized form

$$\frac{\partial p}{\partial t} = \underbrace{\frac{\partial^2 p}{\partial x^2}}_{\text{dispersal}} + \overbrace{\frac{cph}{b(1+ch)}}^{\text{benefit from predation}} - \underbrace{\frac{p}{ab}}_{\text{death}}, \qquad \boxed{\text{predators}} \tag{18a}$$

$$\frac{\partial h}{\partial t} = \underbrace{\delta \frac{\partial^2 h}{\partial x^2}}_{\text{dispersal}} + \overbrace{h(1-h)}^{\text{logistic growth}} - \underbrace{\frac{cph}{1+ch}}_{\text{predation}}. \qquad \boxed{\text{prey}} \tag{18b}$$

The scaled predator and prey densities p and h, respectively, are functions of space, x, and time, t. The omitted nondimensionalization means that parameters a, b, c, δ correspond to ratios of ecological quantities. a is the ratio of predator birthrates and death rates, b is the ratio of prey and predator birthrates, c is the product of prey carrying capacity and a rate associated with how fast prey consumption saturates as the number of prey increases, and δ is the ratio of prey and predator disperal coefficients. For a full model description see, for example, [30].

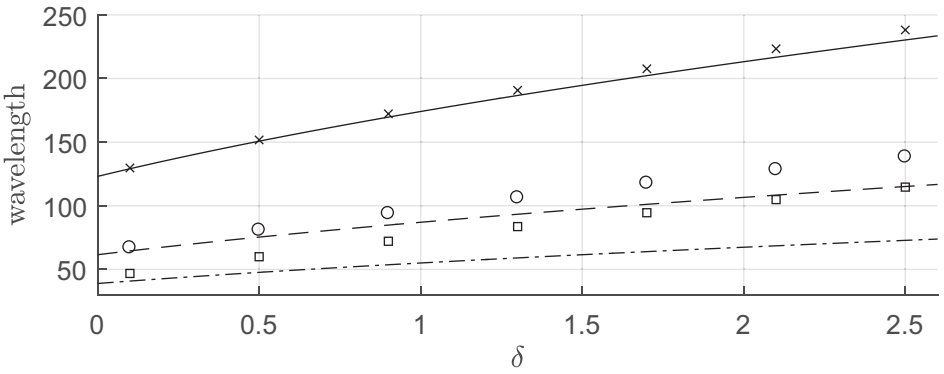

FIG. 2. *A plot to show the relationship between the wavelength of PTWs generated in* (18) *with the diffusion coefficient, δ. Points and lines indicate numerical simulation and analytic approximation, respectively. Parameter values are set to a = 3 and b = 4, giving a Hopf bifurcation point at $c_{crit} = 2$. We consider three different values of c:c = 3 (dot-dashed line and squares), c = 2.4 (dashed line and circles), and c = 2.1 (solid line and crosses)—to show the convergence of the analytic approximation to the numerical simulation as the Hopf bifurcation point is approached.*

There exists one coexistence steady state $(p, h) = (p_s, h_s)$, where $h_s = 1/c(a-1)$ and $p_s = ah_s(1-h_s)$. The Jacobian at (p_s, h_s) is then given by

$$\mathbf{J} = \begin{pmatrix} 0 & \dfrac{ac-c-1}{acb} \\ -\dfrac{1}{a} & \dfrac{ac-a-c-1}{ac(a-1)} \end{pmatrix}.$$

One can easily see that the upper left entry is a zero because the rate of change of predator population density is linear in p, neglecting spatial terms. Let c be our control parameter without loss of generality. At criticality, we see that the bottom right entry is forced to be zero by definition, with the critical value of the parameter given by $c_{\text{crit}} = (a+1)/(a-1)$, and so we have satisfied Theorem 3.1(ii).

In a similar way, we obtain a normal form reduction of λ-ω type if, for arbitrary functions $g_p, g_h : \mathbb{R} \to \mathbb{R}$, either the predator kinetics have the form $p \cdot g_p(h)$ like (18a) or the prey kinetics have the form $h \cdot g_h(p)$. In such cases, we can make predictions about PTWs via (3)–(5), noting the scalings made in section 2. Figure 2 illustrates the effect of dispersal on the wavelength of PTWs. Close to the Hopf bifurcation, the theory describes PTWs well, and analytic predictions match numerical simulations accordingly. Farther away, accuracy is lost as PTWs become larger and less sinusoidal. Theorem 3.1(ii) turns out to be a common feature of many predator–prey models, but the remainder of this paper considers the more general case when (1) satisifes none of the conditions in Theorem 3.1, with the aim of giving a comprehensive method for studying low-amplitude PTW solutions generated by invasion.

4. Amplitude behind invasion in the CGLE. As discussed in section 2, the normal form of (1) in general is the CGLE. Here, we return to the standard x and t notation for the analysis of (12). The CGLE is particularly well studied in the physics community due to its rich dynamics and varied applications [2]. One of the simplest pattern structures that one can generate are PTWs (sometimes called plane waves) given by

$$W = r_0 e^{i(qx+\omega t)}, \tag{19}$$

where $r_0^2 = 1 - q^2 > 0$ and $\omega = (\beta - \alpha)q^2 + \alpha$. This family of solutions is effectively parametrized by the amplitude of the PTW, and so in this section we aim to derive an amplitude equation corresponding to an invasion. Let us first be more precise about what we mean by an invasion. In ecological terms, we want a prey-only environment with a small introduction of predators near the edge of the habitat. This prey-only environment would be the unstable steady state of the predator–prey model; however, the CGLE has a zero unstable steady state obtained via a recentering in the normal form calculation. Mathematically, for some small $p \in \mathbb{R}$, we consider initial conditions of the form

$$W(x,0) = \begin{cases} p, & x = 0, \\ 0, & x > 0, \end{cases} \tag{20a}$$

on a semi-infinite domain $[0, \infty)$. The physical interpretation becomes apparent when one considers the complex counterparts that make up W; $\mathrm{Re}(W)$ and $\mathrm{Im}(W)$ can be interpreted as predator and prey equations, respectively. We specify boundary conditions as

$$\frac{\partial W}{\partial x} = 0 \text{ at } x = 0 \quad \text{and} \quad W \to 0 \text{ as } x \to \infty; \tag{20b}$$

however, numerical simulations show that the left-hand boundary condition affects the behavior of the solution only locally so that one may consider a different condition at $x = 0$ without affecting the generated PTWs.

To simplify analysis, we represent the complex amplitude W in terms of its real amplitude and phase,

$$r_t = r_{xx} - \beta\left(r\theta_{xx} + 2r_x\theta_x\right) - r\theta_x^2 + r(1 - r^2) \tag{21a}$$

$$\theta_t = \theta_{xx} + \beta\left(\frac{r_{xx}}{r} - \theta_x^2\right) + \frac{2r_x\theta_x}{r} - \alpha r^2, \tag{21b}$$

by letting $r = |W|$ and $\tan(\theta) = \mathrm{Im}(W)/\,\mathrm{Re}(W)$. Observing numerical simulations of r (Figure 3(a)) reveals a transition wave moving across the domain in the positive x direction, which changes the amplitude of the solution from zero to that of the generated PTW. One would not expect the same behavior when plotting θ, but previous analysis of the CGLE, for example, [2] (and also of the λ-ω equations [14]), prompts us to consider the phase gradient $\psi := \theta_x$, plotted in Figure 3(b). A transition wave in ψ can clearly be seen moving in parallel with that of r, and so we seek a traveling wave solution of the form $r(x,t) = \tilde{r}(x - ct)$ and $\psi(x,t) = \tilde{\psi}(x - ct)$, which implies $\theta(x,t) = \tilde{\Psi}(x,t) + f(t)$, where $\tilde{\Psi}$ is some indefinite integral of $\tilde{\psi}$ and f is a function to be determined. We get two second-order ordinary differential equations,

$$\tilde{r}'' + c\tilde{r}' + \tilde{r} - \tilde{r}^3 - \tilde{r}\tilde{\psi}^2 - \beta\left(\tilde{r}\tilde{\psi}' + 2\tilde{r}'\tilde{\psi}\right) = 0$$

$$\tilde{\psi}' + c\tilde{\psi} - \alpha\tilde{r}^2 + \frac{2\tilde{r}'\tilde{\psi}}{\tilde{r}} - \beta\left(\tilde{\psi}^2 - \frac{\tilde{r}''}{\tilde{r}}\right) - f'(t) = 0,$$

where a prime denotes differentiation with respect to $z = x - ct$. We define a new parameter $\phi = -\tilde{r}'/\tilde{r}$, following, for example, [42], in order to reduce the system to three first-order differential equations,

$$r' = -r\phi, \tag{22a}$$

$$\phi' = \phi^2 - \beta(\psi' - 2\phi\psi) - \psi^2 - c\phi + 1 - r^2, \tag{22b}$$

$$\psi' = f'(t) + \beta(\psi^2 - \phi^2 + \phi') + 2\phi\psi - c\psi + \alpha r^2, \tag{22c}$$

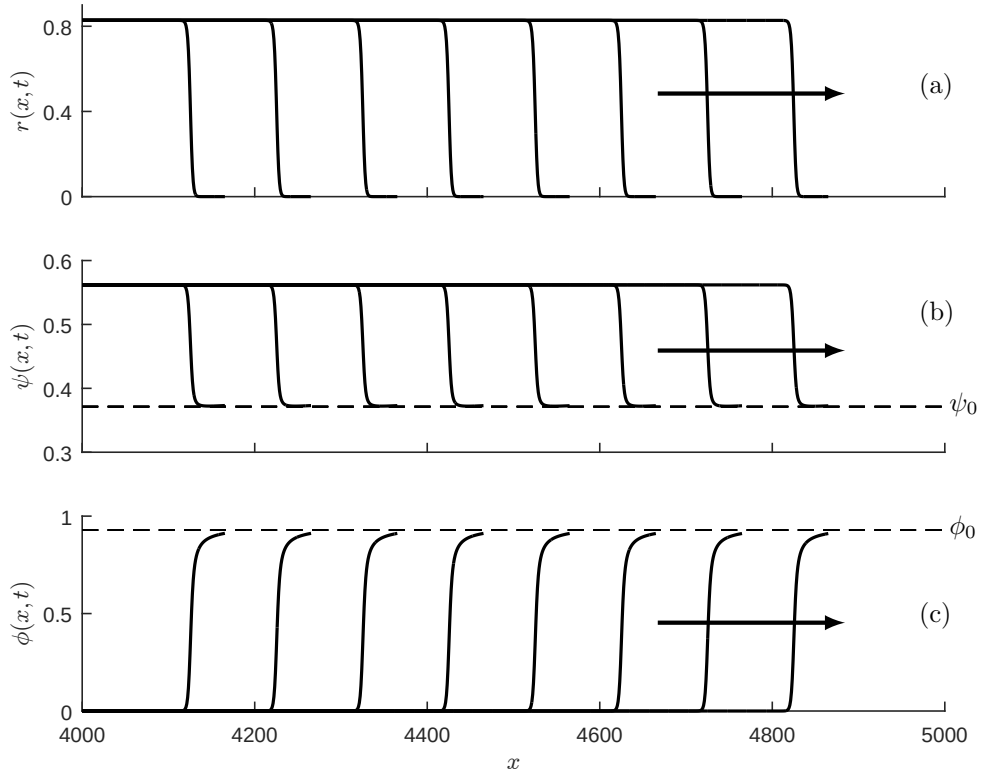

FIG. 3. *Typical solutions for* (a) $r(x,t)$, (b) $\psi(x,t) = \theta_x$, *and* (c) $\phi(x,t) = r_{xx}/r$. *We plot the solution at equally spaced time intervals, revealing a transition wave that moves across the domain in the positive* x *direction. Ahead of the wave front,* $r \to 0$, $\psi \to \psi_0$, *and* $\phi \to \phi_0$; *constants that are easily determined analytically, the details of which can be found in the text. The constant value behind the transition front in* (a), (b), *and* (c) *corresponds to a particular PTW, selected by an invasion given by* (20). *We use parameter values* $\alpha = 1$, $\beta = 0.4$ *and plot solutions until* r *is of the order* 10^{-15}. *The amplitude of periodic traveling waves generated by an invasion (behind the wave front in* (a)*) can be expressed in terms of parameter values as* (27). *This formula gives the amplitude as* 0.827 *to three significant figures.*

where tildes have been dropped. Figure 3 illustrates how all variables tend toward constant values, $r \to 0$, $\psi \to \psi_0$, and $\phi \to \phi_0$ as $x \to \infty$, where ψ_0 and ϕ_0 are constants. Examining the behavior of the system for large x will give us an expression for f, allowing us to calculate the steady states of (22) in terms of α and β.

The quantities ϕ_0, ψ_0, and c can be derived using the theory of front propagation into unstable steady states, for which a detailed review has been collated by van Saarloos [43]. Equation (12) has a linearly unstable steady state at $W = 0$, implying that our localized initial condition (20a) will grow and spread in the positive x-direction, as we have seen. There are two classes of traveling front that can develop: either a "pulled" front or a "pushed" front, both of which travel at different speeds in the limit $t \to \infty$. Our initial conditions are sufficiently "steep" (see [43]) for a pulled front to develop, and therefore c is the asymptotic linear spreading speed associated with the dynamical equations obtained by linearizing the CGLE. It is easily calculated from

the linear dispersion relation along with ϕ_0 and ψ_0. If one decomposes W into Fourier modes, we can write

$$\tilde{W}(k,t) = \int_{-\infty}^{\infty} W(x,t)e^{-ikx}\mathrm{d}x$$

and calculate the linear dispersion relation, $\omega(k)$ via the substitution of the ansatz,

$$\tilde{W}(k,t) = \bar{W}(k)e^{-i\omega(k)t}, \tag{23}$$

giving $\omega(k) = (\beta - i)k^2 + i$. The inverse Fourier transform and (23) can then be used to write

$$W(x,t) = \frac{1}{2\pi}\int_{-\infty}^{\infty} \bar{W}(k)e^{ikx - i\omega(k)t}\mathrm{d}x, \tag{24}$$

where $\bar{W}$ is just the Fourier transform of the initial condition.

Consider two observers initially located at $x = 0$ who move off in the positive x-direction along with the wave front. The first observer is moving at some speed greater than c and so will eventually see the unstable zero steady state that is being invaded, whereas the observer moving at some speed less than c will eventually see the invasive stable steady state, which in our case takes the form of PTWs. If we consider a moving frame of reference $z = x - ct$, the front should neither grow nor decay. Then (24) becomes

$$W(z,t) = \frac{1}{2\pi}\int_{-\infty}^{\infty} \bar{W}(k)e^{ikz - i[\omega(k) - ck]t}dk,$$

which can be evaluated using the method of steepest descent (saddle point approximation) due to the large time limit. The saddle point, k^*, is given by

$$\left.\frac{\mathrm{d}[\omega(k) - ck]}{\mathrm{d}k}\right|_{k^*} = 0 \qquad \Longrightarrow \qquad c = \left.\frac{\mathrm{d}\omega(k)}{\mathrm{d}k}\right|_{k^*} = 2(\beta - i)k^*. \tag{25}$$

Furthermore, the dominant term in the integral becomes $e^{i[\omega(k^*) - ck^*]t}$ because of the expansion in the exponent associated with the saddle point approximation. Hence, to ensure that this term neither grows nor decays, we also have the condition

$$\mathrm{Im}(\omega(k^*)) - c\,\mathrm{Im}(k^*) = 0,$$

which together with (25) gives us an expression for the asymptotic speed of the transition front. The values of ψ_0 and ϕ_0 are the real and imaginary parts of the saddle point, respectively, and so we obtain the expressions

$$c = 2\sqrt{1 + \beta^2}, \qquad \phi_0 = \frac{1}{\sqrt{1 + \beta^2}}, \qquad \psi_0 = \frac{\beta}{\sqrt{1 + \beta^2}}. \tag{26}$$

Returning to (22), we let $x \to \infty$, implying that $r \to 0$, $\phi \to \phi_0$, $\psi \to \psi_0$, and the speed of the wave front approaches c, so we calculate via (26) that $f'(t) = \beta$; it is not necessary to calculate $f(t)$ in order to proceed. The steady states $(r, \phi, \psi) = (r_s, \phi_s, \psi_s)$ must satisfy $r_s\phi_s = 0$ from (22a). $r_s = 0$ is the steady state ahead of the wave front, and so we assume $\phi_s = 0$ with $r_s = r_0 > 0$. The steady state behind the

wave front must then satisfy $1 - r_0^2 - \psi_s^2 = 0$ and $\beta(1 + \psi_s^2) - c\psi_s + \alpha r_0^2 = 0$, and by solving these equations we obtain the amplitude

$$r_0 = \left[\frac{2}{(\alpha - \beta)^2} \left(\sqrt{(1 + \alpha^2)(1 + \beta^2)} - (1 + \alpha\beta) \right) \right]^{\frac{1}{2}} \tag{27}$$

of PTWs given by (19), generated by an invasion described by (20), which is the analogue of (5).

Many results derived about PTWs generated in the CGLE are hinged on the assumption that the amplitude is a known parameter value. In empirical data sets, this is an unlikely premise due to the difficulties in recording spatiotemporal data. In numerical simulations of a mathematical model, the calculation of an amplitude is more feasible, though an accurate reading can require large computation times and would need to be repeated with each new set of parameter values. In both cases, it is a necessary requirement that PTWs have already been generated, though from simulations (see Figure 7) one can see that a certain amount of time is needed before one starts to observe oscillatory behavior. The use of (27) allows one to predict PTWs analytically from the system's initial conditions rather than examining existing PTWs in order to derive further characteristics. This is of particular benefit to ecologists making predictions about newly invading species. The following section describes how one can use (27) to determine the stability of PTWs with respect to model parameter values.

5. Stability of PTWs in the CGLE. For certain parameter values, irregular wakes occur behind invasion (see Figure 4), making the notion of an amplitude irrelevant. In order for (27) to be of any use, we must be able to say in terms of our choice of parameters whether one will generate stable PTWs or spatiotemporal irregularity. Stability can be loosely described as follows: a solution is stable if any small perturbation decays over time. In contrast, a solution is unstable if some small perturbation grows over time. To investigate the stability of PTWs

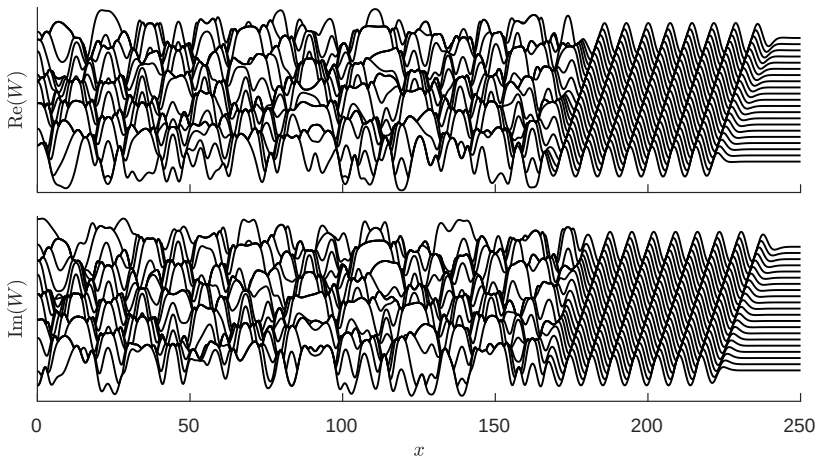

FIG. 4. *An illustration of instability of PTWs generated in the CGLE by an invasion of the unstable zero steady state. Numerical solutions of* (18) *are plotted as functions of space, x, at successive times, t. The vertical separation between plots is proportional to the time interval, with time increasing up the plot. A band of PTWs can be seen immediately behind the invasion, before waves destabilise into spatiotemporal irregularity. Parameter values are $\alpha = 5$, $\beta = 0.4$, and initial/boundary conditions are given by* (20).

in the CGLE, we consider (21) and linearize about the PTW solution given by $(r,\theta) = (r_0, \sqrt{1-r_0^2}x + \left[(\alpha-\beta)r_0^2+\beta\right]t)$, yielding a set of equations for small perturbations $\hat{r}$, $\hat{\theta}$,

$$\hat{r}_t = \hat{r}_{xx} - \beta r_0 \hat{\theta}_{xx} - 2\sqrt{1-r_0^2}(\beta\hat{r}_x + r_0\hat{\theta}_x) - 2r_0^2\hat{r} \tag{28a}$$

$$\hat{\theta}_t = \hat{\theta}_{xx} - \frac{\beta\hat{r}_{xx}}{r_0} + 2\sqrt{1-r_0^2}\left(\frac{\hat{r}_x}{r_0} - \beta\hat{\theta}_x\right) - 2\alpha r_0\hat{r}, \tag{28b}$$

with constant coefficients. In a standard way, one then looks for solutions of (28) in the form $(\hat{r},\hat{\theta}) = (\bar{r},\bar{\theta})\exp(\lambda t + ikx)$. After some manipulation, one obtains the dispersion relation as

$$\begin{aligned} 0 = \mathcal{D}(\lambda,k) :&= \lambda^2 + 2\lambda\left[k^2 + 2ik\beta\sqrt{1-r_0^2} + r_0^2\right] \\ &\quad + k^2\left[(1+\beta^2)k^2 + (4\beta^2 + 2\alpha\beta + 6)r_0^2 + 4(1-\beta^2)\right] \\ &\quad + 4ik(\beta-\alpha)r_0^2\sqrt{1-r_0^2}. \end{aligned} \tag{29}$$

For stability, we must take $k \in \mathbb{R}$ and consider the set containing values of λ such that $\mathcal{D}(\lambda,k) = 0$; this is known as the "essential spectrum." Note that the essential spectrum with respect to (29) necessarily goes through the origin for all r_0 since $\mathcal{D}(0,0) = 0$, reflecting the neutral stability of waves to translation. Therefore, the condition for stability is that $\mathrm{Re}(\lambda) < 0$ for all λ in the essential spectrum, except $\lambda = 0$. Ideally, one would like to derive an analytic condition for stability in terms of parameter values, analogous to (5) for the λ-ω equations, though in the CGLE this is possible only in the small k limit.

If one expands the growth rate λ in powers of k, giving

$$\lambda = -2iq(\alpha-\beta)k - \left[1 + \alpha\beta - \frac{2q^2(1+\alpha^2)}{r_0^2}\right]k^2 + O(k^3), \tag{30}$$

one can then easily see that PTWs are stable to long-wave perturbations when

$$1 + \alpha\beta - \frac{2(1-r_0^2)(1+\alpha^2)}{r_0^2} > 0, \tag{31}$$

which is known formally as the Eckhaus criterion [8]. In many situations, Eckhaus stability does indeed imply that PTWs are stable. A more rigorous stability analysis has been carried out by Matkowsky and Volpert [19] that considers the case when (31) is not sufficient for stability. In particular, they demonstrate that for smaller values of r_0, waves can destabilize for larger values of k—this is sometimes known as a "Hopf"-type instability, illustrated in Figure 5. Figure 5(a) demonstrates, in parameter space, how Eckhaus curves given by (31) can differ significantly from the true stability boundary, which we calculate numerically. By setting $r_0 = 0.72$, we select PTWs with amplitude small enough for destabilization via Hopf instability. Since $k = 0$ when $\lambda = 0$, as mentioned, small values of k correspond to the elements of the essential spectrum near the origin in the complex λ plane; these values determine whether a wave is Eckhaus stable. Figures 5(b)–(d) are plots of the essential spectrum for a Hopf instability; in particular, Figure 5(c) is the spectrum of an unstable wave that is Eckhaus stable, demonstrating that the Eckhaus criterion is valid only in the limit $k \to 0$. For the models considered in this paper, we always have the Eckhaus case, but in general one must be careful to rule out the possibility of a Hopf destabilization mechanism as shown in Figure 5.

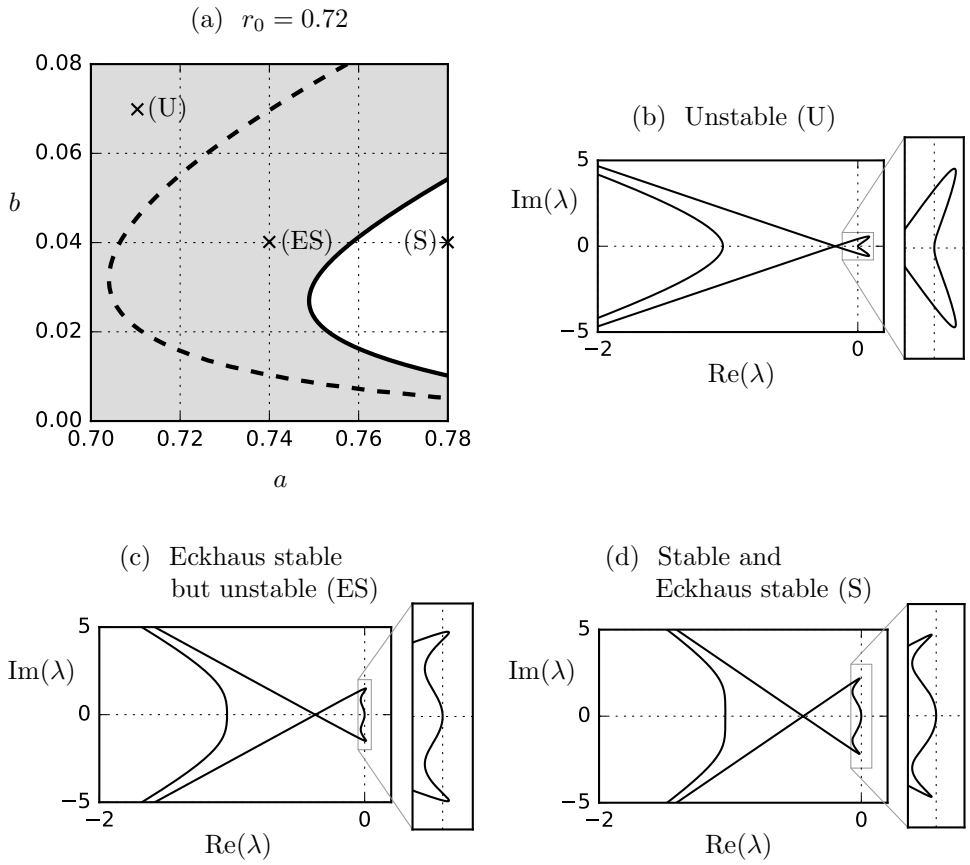

FIG. 5. *Plots to illustrate a Hopf-type instability in the CGLE in terms of ecological parameters relating to* (32) *defined in section* 7*, with* $\delta = -0.68$ *(note this is an ecologically insignificant parameter choice). In* (a)*, we can see the difference in the Eckhaus curve (dashed line), calculated using* (31)*, and the true stability line (solid line), which is calculated numerically and separates unstable (shaded) and stable (white) regions of the a-b parameter plane.* (b)–(d) *are plots of essential spectra for different parameter values. Point (U) in* (a) *represents parameter values* $a = 0.71$*,* $b = 0.07$*, and gives the spectrum in* (b)*, implying unstable (and Eckhaus unstable) PTWs. Similarly, point (ES) represents parameters* $a = 0.74$*,* $b = 0.04$*, and is associated with spectrum* (c)*. In this case,* $\mathrm{Re}(\lambda) < 0$ *close to the origin, implying the PTW is stable to perturbations with large wavelength but unstable overall due to larger* k *values located away from the origin in the complex* λ *plane. Point (S) represents a PTW with parameter values* $a = 0.78$*,* $b = 0.03$*, that is stable, as seen in the corresponding spectrum* (d)*.*

6. Absolute and convective instabilities. We now focus on unstable PTWs, distinguishing between absolute and convective instabilities. If a perturbation grows in time at every fixed point in the domain, we say the solution is "absolutely unstable." The issue is that in a spatially dependent system, a perturbation may move in space while it grows, meaning that the perturbation may decay at the point at which it is applied but grow overall. If perturbations decay at every fixed point but the overall norm of the perturbation grows, then we say the solution is "convectively unstable." In our specific case, a convective instability allows a band of PTWs to be seen behind invasion, before they appear to destabilize. This is because, for an invasion, we consider a finite domain with separated boundary conditions so that perturbations

moving away from one boundary do not reenter at the other. Figure 4 illustrates how a fixed-width band of PTWs is generated behind the invasion front. From an ecological viewpoint, one would wish to be able to predict whether PTWs observed in practice will eventually destabilize.

A few methods exist that calculate whether an unstable steady state is absolutely or convectively unstable, some of which are very complicated [6, 37], and so we proceed with a method that uses the notion of an "absolute spectrum," a term coined by Sandstede and Scheel [28]. To explain the absolute spectrum, we refer back to the dispersion relation, $\mathcal{D}(\lambda, k) = 0$, as given by (29)—a fourth-order polynomial in k. Now though, it is necessary to let $k \in \mathbb{C}$. For a given λ, we obtain four roots for k that we label $k_i(\lambda)$ $(i = 1, 2, 3, 4)$ such that

$$\mathrm{Im}(k_1) \leq \mathrm{Im}(k_2) \leq \mathrm{Im}(k_3) \leq \mathrm{Im}(k_4).$$

For a system of two coupled reaction-diffusion equations (in our case the real and imaginary parts of (12)), the "absolute spectrum" is the set of λ values such that $\mathrm{Im}(k_2) = \mathrm{Im}(k_3)$ (for details of this, we refer the reader to the proofs in [28]). Whether a solution is absolutely or convectively unstable can be determined by the branch points in the absolute spectrum [28]—if all branch points have $\mathrm{Re}(\lambda) < 0$, the solution is convectively unstable, whereas if there exists a branch point with $\mathrm{Re}(\lambda) > 0$, the solution is absolutely unstable. In principal, the absolute spectrum can cross into the right-hand half of the complex plane even when all branch points are in the left-hand half; the solution would then have "remnant" instability [28, 34], with growing perturbations traveling in both space directions. This is extremely rare—we know of only one documented example [24]—and we have seen no evidence for behavior of this type in our simulations. Figure 6 shows the division of the parameter plane into absolutely and convectively unstable cases via the calculation of branch points of the absolute spectrum.

7. Example: The Leslie-May model. We now put the theory described in sections 4–6 into practice via an example. A well-established model, sometimes known as the Leslie [18] or May [20] model for predators, $p(x, t)$, and prey, $h(x, t)$, can be written in its nondimensionalized form as

$$\frac{\partial p}{\partial t} = \underbrace{\frac{\partial^2 p}{\partial x^2}}_{\text{dispersal}} + \overbrace{cp}^{\text{benefit from predation}} - \underbrace{\frac{cp^2}{h}}_{\text{death}}, \qquad \boxed{\text{predators}} \tag{32a}$$

$$\frac{\partial h}{\partial t} = \underbrace{\delta \frac{\partial^2 h}{\partial x^2}}_{\text{dispersal}} + \overbrace{h(1-h)}^{\text{logistic growth}} - \underbrace{\frac{aph}{b+h}}_{\text{predation}}, \qquad \boxed{\text{prey}} \tag{32b}$$

where a, b, c, and δ are positive constants from which we, again, select c as our control parameter. There are two coexistence homogeneous steady states, and so, without loss of generality, we consider

$$p_s = \frac{1}{2}\left(1 - a - b + \sqrt{((1-a-b)^2 + 4b)}\right), \qquad h_s = p_s.$$

Although the Leslie-May model appears similar to (18), the key difference is in the predator equation; due to a logistic-type growth of predators, the kinetic part

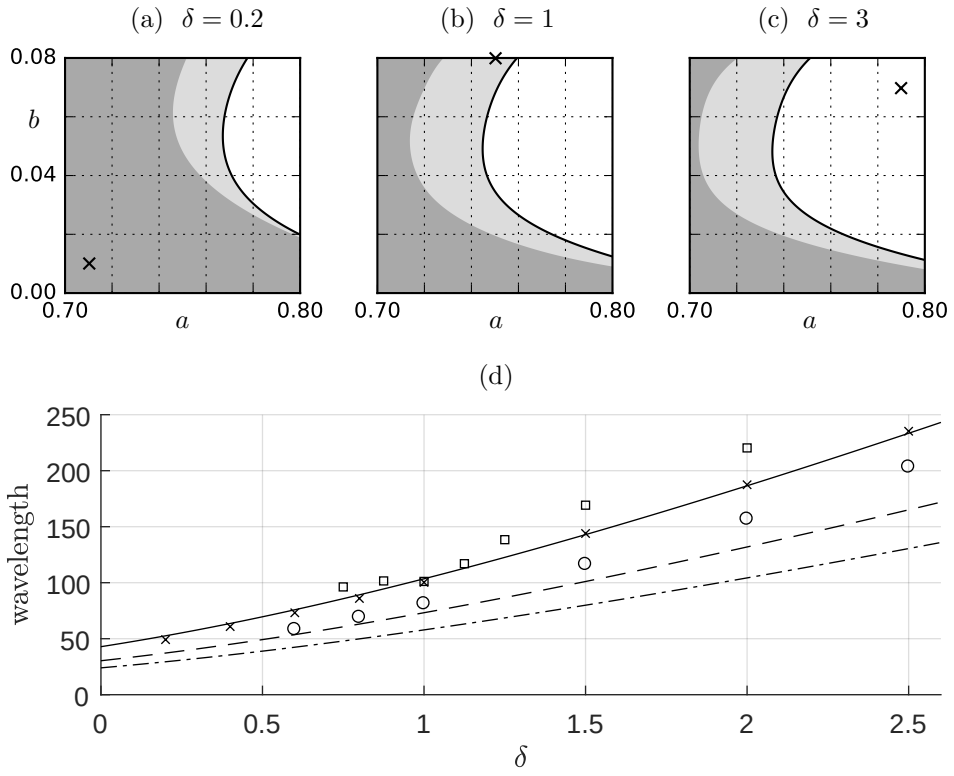

FIG. 6. *The effect of diffusion on PTWs generated by invasion in* (32). (a)–(c) *show the stable (white) and unstable (shaded) regions of the parameter space, separated by the Eckhaus stability boundary (black line) calculated using* (31)*, for different values of the diffusion coefficient,* δ*. The light shaded region represents convective instability in the generated PTWs (see section* 6*) and indicates that a band of PTWs will be observed before destabilisation. The dark shaded region represents absolutely unstable behaviour for which no PTWs are observed. The absolute stability boundary is calculated numerically by finding branch points in the absolute spectrum (see section* 6 *for details).* (b) *represents the* λ*–*ω *case discussed in sections* 1 *and* 3*. Crosses relate to Figure* 7*. In* (d)*, we plot wavelength against* δ *to compare analytic predictions (lines) with numerical simulations (points) for different values of the control parameter,* c*. We set* $a = 0.76$*,* $b = 0.04$*, giving a Hopf bifurcation point at* $c_{crit} \approx 0.29$ *(see* (33)*), below which cyclic behavior occurs. We plot for* $c = 0.24$ *(solid line and crosses),* $c = 0.19$ *(dashed line and circles), and* $c = 0.13$ *(dot-dashed line and squares). As we approach* c_{crit}*, our analytic predictions converge to numerical simulations.*

of (32a) is no longer linear in p. To be clear, one can calculate the associated Jacobian as

$$\mathbf{J} = \begin{pmatrix} -c & c \\ -\dfrac{ah_s}{(b+h_s)} & 1 - 2h_s - \dfrac{ap_s}{b+h_s} + \dfrac{ap_s h_s}{(b+h_s)^2} \end{pmatrix},$$

which, when evaluated at the Hopf bifurcation point

$$c_{crit} = 1 - 2h_s - \frac{ap_s}{b+h_s} + \frac{ap_s h_s}{(b+h_s)^2}, \tag{33}$$

no longer satisfies Theorem 3.1(ii) in section 3. Therefore, when Theorem 3.1(i) does not hold, we must proceed by reducing (32) to the CGLE. We do not give the normal

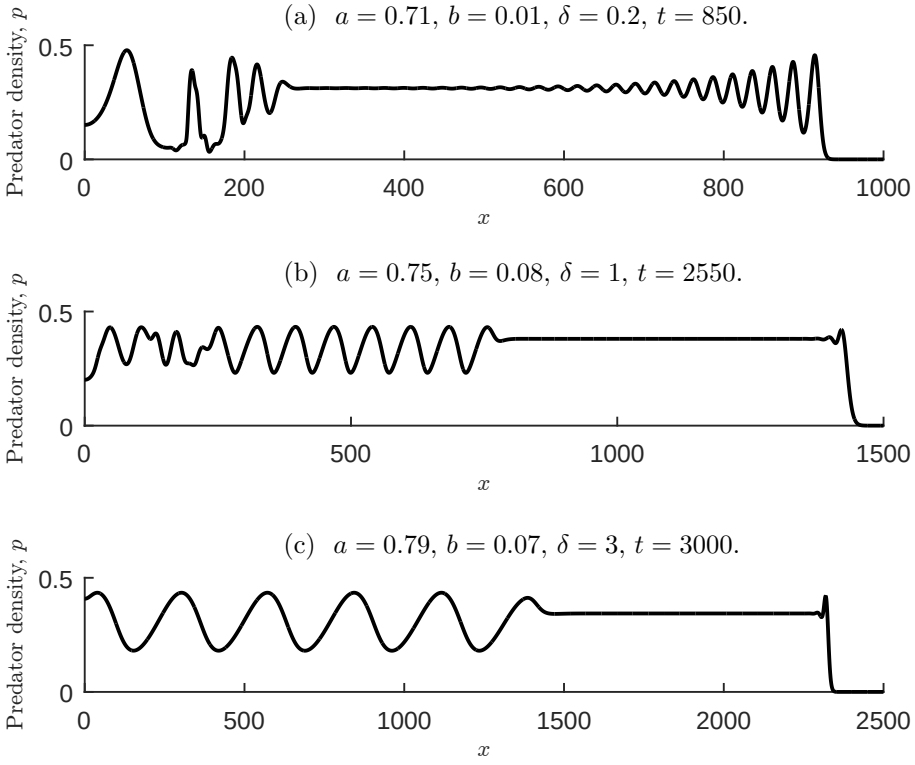

FIG. 7. *Numerical simulations to show the effect of parameter values, illustrated in Figure* 6*, on stability. We fix* $c - c_{crit} = 0.05$ *so that we are a constant distance from the Hopf bifurcation. Note that* (a) *is related to parameters represented by a cross in Figure* 6(a) *and, similarly, that* (b) *and* (c) *relate to Figures* 6(b) *and* 6(c)*, respectively. In* (a)*, the selected PTW is absolutely unstable, and irregular behavior is observed immediately behind invasion due to stationary modes. In* (b)*, the selected PTW is convectively unstable, allowing a band of PTWs to develop before perturbations grow large enough to be observed at* $x = 220$*. In* (c)*, a stable PTW is selected.*

form expressions explicitly since they are long and awkward, but they can be easily calculated using a computer algebra package via (13), giving us $\alpha = \alpha(a, b)$ and $\beta = \beta(a, b, \delta)$. These expressions can be substituted into (27), allowing one to specify the PTW selected by invasion from (19) in terms of the original model parameters. We have investigated a wide range of ecologically significant parameter choices and find, in all cases, that PTWs destabilize via an Eckhaus instability so that (31) determines stability. For other methods of wave generation, PTWs could destabilize via Hopf instability, and one would have to calculate stability numerically (see section 5)—we give an example of this for (32) in Figure 5(a) for a fictional method of wave generation that generates PTWs of amplitude $r_0 = 0.72$.

Figures 6(a)–(c) use (31) to calculate stable and unstable regions of the parameter plane. In addition, we calculate absolutely unstable regions (where spatiotemporal irregularity is observed immediately behind invasion) and convectively unstable regions (where PTWs are observed but then destabilize after some time) by calculating branch points in the absolute spectrum. Assuming that PTWs are observed, we can make predictions about their characteristics: Figure 6(d) demonstrates the effect of δ on the wavelength while highlighting the importance of being close to the Hopf

bifurcation. Close to c_{crit}, our predictions agree well with numerical simulations, but as c moves away from c_{crit}, they become less accurate, though, in accordance with normal form theory.

8. Discussion. Our amplitude equation (27) enables us to specify explicit solution forms for a more general class of ecological models (1), giving accurate predictions of PTW characteristics near a Hopf bifurcation. We have shown that dispersal has a significant effect on the general stability of PTWs and for unstable waves employed the notion of absolute and convective instabilities to predict the existence of a band of waves prior to destabilization into spatiotemporal irregularity. Furthermore, by combining theory from [35] with the results in this paper, one can calculate the bandwidth of a band of PTWs.

We suggest three directions for future work:

- Large-amplitude PTWs: Our work has assumed that PTWs must necessarily be of the small-amplitude type by fixing a control parameter close to the Hopf bifurcation point. Ecologists, in general, would be interested in large-amplitude PTWs that have a more significant impact on the surrounding ecosystem. This is the natural direction for future work on PTW selection—little has been done in this area, with the exception of recent work by Merchant and Nagata [21, 22], who developed a new method of PTW prediction that retains accuracy further from the Hopf bifurcation by assuming the existence of a front between the spatially homogeneous steady state and the selected PTW.
- Nonlocal dispersal: For many natural populations, diffusion is considered to be a crude representation of movement, failing to capture instances of rare long-distance dispersal events. Recent work [32, 33], instead, uses spatial convolution with a dispersal kernel, which is more accurate in many systems. In [32, 33], it is assumed throughout that parameters are close to a Hopf bifurcation and that dispersal terms are the same for predators and prey, enabling one to approximate the model via the λ-ω equations. Instead, one could allow dispersal coefficients to vary, resulting in a CGLE normal form and allowing one to apply the results in this paper to models with nonlocal dispersal. A much harder problem, though, would be to study the dynamics for different dispersal kernels, which would give a completely different and, likely, more complicated normal form equation.
- Two-dimensional perturbations: Our focus with regards to the stability of PTWs has been on one-dimensional patterns. In reality, ecological systems are more accurately represented in two space dimensions, the implication being that PTWs that are stable to one-dimensional perturbations may or may not be stable when trivially extended as striped patterns. This is because of additional transverse two-dimensional perturbations. Siero et al. [36] have done work in this area with respect to banded vegetation patterns observed in semiarid desert regions. The authors identify that the resilience of these striped patterns is greater on a steeper incline by numerically computing stability regions, and show that the destabilization process leads to "dashed" vegetation patterns before desertification. The consideration of two-dimensional perturbations in relation to PTWs in cyclic populations could reveal interesting new pattern formations that are as yet undiscovered due to a lack of empirical data.

REFERENCES

[1] A. Angerbjörn, M. Tannerfeldt, and H. Lundberg, *Geographical and temporal patterns of lemming population dynamics in fennoscandia*, Ecography, 24 (2001), pp. 298–308.

[2] I. S. Aranson and L. Kramer, *The world of the complex Ginzburg-Landau equation*, Rev. Mod. Phys., 74 (2002), pp. 99–143.

[3] V. N. Biktashev and M. A. Tsyganov, *Spontaneous traveling waves in oscillatory systems with cross diffusion*, Phys. Rev. E, 80 (2009).

[4] O. N. Bjørnstad, M. Peltonen, A. M. Liebhold, and W. Baltensweiler, *Waves of larch budmoth outbreaks in the European Alps*, Science, 298 (2002), pp. 1020–1023.

[5] M. J. Brandt and X. Lambin, *Movement patterns of a specialist predator, the weasel mustela nivalis exploiting asynchronous cyclic field vole microtus agrestis populations*, Acta Theriologica, 52 (2007), pp. 13–25.

[6] R. J. Briggs, *Electron-Stream Interaction with Plasmas*, MIT Press, Cambridge, MA, 1964.

[7] A. N. Cohen, J. T. Carlton, and M. C. Fountain, *Introduction, dispersal and potential impacts of green crabs carcinus-maenas in San-Fransisco Bay, California*, Marine Biol., 122 (1995), pp. 225–237.

[8] W. Eckhaus, *Studies in Non-Linear Stability Theory*, vol. 6, Springer, Berlin, Heidelberg, 1965.

[9] I. R. Epstein and K. Showalter, *Nonlinear chemical dynamics: Oscillations, patterns and chaos*, J. Phys. Chem., 100 (1996), pp. 13132–13147.

[10] J. Guckenheimer and P. Holmes, *Nonlinear Oscillations, Dynamical Systems, and Bifurcations of Vector Fields*, 42, Springer-Verlag, New York, 1983.

[11] C. Hauzy, F. D. Hulot, and A. Gins, *Intra and interspecific density-dependent dispersal in an aquatic preypredator system*, J. Anim. Ecol., 76 (2007), pp. 552–558.

[12] J. A. Hicke et al., *Effects of biotic disturbances on forest carbon cycling in the United States and Canada*, Global Change Biol., 18 (2012), pp. 7–34.

[13] A. L. Kay and J. A. Sherratt, *Spatial noise stabilizes periodic wave patterns in oscillatory systems on finite domains*, SIAM J. Appl. Math., 61 (2000), pp. 10131041.

[14] N. Kopell and L. N. Howard, *Plane wave solutions to reaction-diffusion equations*, Stud. Appl. Math., 52 (1973), pp. 291–328.

[15] Y. Kuramoto, *Chemical Oscillation, Waves and Turbulence*, Springer Series in Synergetics 19, Springer, Berlin, 1984.

[16] Y. Kuznetsov, *Elements of Applied Bifurcation Theory*, 3rd ed., Springer-Verlag, New York, 2004.

[17] X. Lambin, D. A. Elston, S. J. Petty, and J. L. MacKinnon, *Spatial asynchrony and periodic travelling waves in cyclic populations of field voles*, Proc. R. Soc. B, 265 (1998), pp. 1491–1496.

[18] P. H. Leslie, *Some further notes on the use of matrices in population dynamics*, Biometrika, 35 (1948), pp. 213–245.

[19] B. J. Matowsky and V. Volpert, *Stability of plane wave solutions of complex Ginzburg-Landau equations*, Quart. Appl. Math., 51 (1993), pp. 265–281.

[20] R. May, *Stability and Complexity in Model Ecosystems*, Princeton University Press, Princeton, NJ, 1974.

[21] S. M. Merchant and W. Nagata, *Wave train selection behind invasion fronts in reaction-diffusion predator-prey models*, Phys. D, 239 (2010), pp. 1670–1680.

[22] S. M. Merchant and W. Nagata, *Selection and stability of wave trains behind predator invasions in a model with non-local prey competition*, IMA J. Appl. Math., 80 (2015), pp. 1155–1177.

[23] A. Morozov, S. Petrovskii, and B.-L. Li, *Spatiotemporal complexity of patchy invasion in a predator-prey system with the allee effect*, J. Theoret. Biol., 238 (2006), pp. 18–35.

[24] J. Rademacher, B. Sandstede, and A. Scheel, *Computing absolute and essential spectra using continuation*, Phys. D, 229 (2007), pp. 166–183.

[25] J. D. M. Rademacher and A. Scheel, *Instabilities of wave trains and Turing patterns in large domains*, Int. J. Bifur. Chaos, 17 (2007), pp. 2679–2691.

[26] E. Ranta and V. Kaitala, *Travelling waves in vole population dynamics*, Geochim. Cosmochim. Acta, 61 (1997), pp. 3503–3512.

[27] M. L. Rosenzweig and R. H. MacArthur, *Graphical representation and stability conditions of predator-prey interactions*, Amer. Naturalist, 97 (1963), pp. 209–223.

[28] B. Sandstede and A. Scheel, *Absolute and convective instabilities of waves on unbounded and large bounded domains*, Phys. D, 145 (2000), pp. 233–277.

[29] J. A. Sherratt, *On the evolution of periodic plane waves in reaction-diffusion equations of λ-ω type*, SIAM J. Appl. Math., 54 (1994), pp. 1374–1385.
[30] J. A. Sherratt, *Periodic travelling waves in cyclic predator prey systems*, Ecol. Lett., 4 (2001), pp. 30–37.
[31] J. A. Sherratt, *Generation of periodic travelling waves in cyclic populations by hostile boundaries*, Proc. R. Soc. Lond. A, 469 (2013).
[32] J. A. Sherratt, *Periodic traveling waves in integrodifferential equations for nonlocal dispersal*, SIAM J. Appl. Dyn. Syst., 13 (2014), pp. 1517–1541.
[33] J. A. Sherratt, *Invasion generates periodic traveling waves (wavetrains) in predator-prey models with nonlocal dispersal*, SIAM J. Appl. Math., 76 (2016), pp. 293–313.
[34] J. A. Sherratt, A. S. Dagbovie, and F. M. Hilker, *A mathematical biologists guide to absolute and convective instability*, Bull. Math. Biol., 76 (2014), pp. 1–26.
[35] J. A. Sherratt, M. J. Smith, and J. D. M. Rademacher, *Locating the transition from periodic oscillations to spatiotemporal chaos in the wake of invasion*, Proc. Natl. Acad. Sci. USA, 106 (2009), pp. 10890–10895.
[36] E. Siero, A. Doelman, M. B. Eppinga, J. D. M. Rademacher, M. Rietkirk, and K. Siteur, *Striped pattern selection by advective reaction-diffusion systems: Resilience of banded vegetation on slopes*, Chaos, 25 (2015).
[37] S. A. Suslov and S. Paolucci, *Stability of non-Boussinesq convection via the complex Ginzburg-Landau model*, Fluid Dyn. Res., 35 (2004), pp. 159–203.
[38] O. Tenow, A. Nilssen, H. Bylund, and O. Hogstad, *Waves and synchrony in epirrita autumnata/operophtera brumata outbreaks.* I. *Lagged synchrony: Regionally, locally and among species*, J. Animal Ecolo., 76 (2007), pp. 258–268.
[39] D. M. Tompkins, A. R. White, and M. Boots, *Ecological replacement of native red squirrels by invasive greys driven by disease*, Ecol. Lett., 6 (2003), pp. 189–196.
[40] P. Turchin, J. D. Reeve, J. T. Cronin, and R. T. Wilkens, *Spatial Pattern Formation in Ecological Systems: Bridging Theoretical and Empirical Approaches*, Spatiotemporal Dynamics in Ecology, Springer and Landes Bioscience, Berlin, 1998, pp. 199–208.
[41] R. Tyson, S. Haines, and K. E. Hodges, *Modelling the Canada lynx and snowshoe hare population cycle: The role of specialist predators*, Theoret. Ecol., 3 (2010), pp. 97–111.
[42] M. van Hecke, *Building blocks of spatiotemporal intermittency*, Phys. Rev. Lett., 80 (1998), pp. 1896–1899.
[43] W. van Saarloos, *Front propagation into unstable states*, Phys. Rep., 386 (2003), pp. 29–222.
[44] E. A. Wieters et al., *Scales of dispersal and the biogeography of marine predator-prey interactions*, Amer. Naturalist, 171 (2008), pp. 405–417.
[45] M. A. Wulder et al., *Surveying mountain pine beetle damage of forests: A review of remote sensing opportunities*, Forest Ecol. Manag., 221 (2006), pp. 27–41.